Journal of Rare Cardiovascular Diseases
ISSN: 2299-3711 (Print) | e-ISSN: 2300-5505 (Online)
www.jrcd.eu
RESEARCH ARTICLE

# Docking-Based Screening of Indanone Analogues Against AChE: A Comprehensive In Silico Investigation

**Sweety*[1], Parveen Yadav2, Ankit Jain[3], Naresh Kalra[1]**
[1]. Faculty of Pharmacy, Lords University, Chikani, Alwar- 301028
[2]. Department of Pharmacy, Sushant University, Gurugram- 122011.
[3]. Amity Institute of Pharmacy, Amity University Punjab, Mohali- 140306.

*Corresponding Author
Sweety

Article History
**Received: 10.10.2025**
**Revised: 24.10.2025**
**Accepted: 05.11.2025**
**Published: 05.12.2025**

Abstract: Indanone derivatives constitute an important class of bioactive molecules known for their acetylcholinesterase (AChE) inhibitory and antioxidant properties. Owing to their aromatic and heterocyclic architecture, indanones possess the structural features necessary for hydrogen bonding, π–π stacking, and hydrophobic interactions within enzymatic active sites. This study investigates the binding affinity, interaction profile, and drug-likeness of 36 literature-reported indanone-based ligands using molecular docking against the target protein (PDB ID: 7E3H). Ligands were optimised using MMFF94 force field and docked using AutoDock Vina, followed by validation through redocking and RMSD evaluation. Docking scores ranged from –10.8 to –13.4 kcal/mol, with Ligands 14, 15, 16, and 33 showing the highest affinities. Detailed 2D/3D interaction analyses revealed that strong inhibitors formed multiple hydrogen bonds, π–π stacking with aromatic residues, and deep hydrophobic interactions with Trp86, Trp286, Tyr341, and Phe residues within the catalytic gorge. ADMET predictions indicated favourable pharmacokinetic properties, low predicted toxicity, and acceptable metabolic profiles for the top-performing ligands. Collectively, the results highlight several promising indanone derivatives as potential lead molecules for further experimental validation and drug development

Keywords: Indanone derivatives; Molecular docking; Acetylcholinesterase inhibition; Antioxidant activity; ADMET predictions..

## INTRODUCTION

Indanone derivatives represent a vital class of heterocyclic compounds exhibiting diverse pharmacological activities, including enzyme inhibition, antioxidant defence, and neuroprotective effects. Structurally, indanones are bicyclic molecules composed of a benzene ring fused to a cyclopentanone moiety. This structural arrangement confers rigidity and π-electron conjugation, allowing indanones to participate in hydrogen bonding and π–π interactions with biological macromolecules. Among their various biological properties, **acetylcholinesterase (AChE) inhibition** and **antioxidant activity** are particularly noteworthy due to their relevance in maintaining cholinergic transmission and preventing oxidative cellular damage. The study of indanone-based AChE inhibitors has thus gained attention for their potential as multifunctional therapeutic scaffolds with free radical scavenging capacity and enzyme modulatory effects [1]

### 1.1 Acetylcholinesterase Inhibition Mechanism of Indanones

Acetylcholinesterase (AChE) is a key enzyme responsible for hydrolysing the neurotransmitter acetylcholine into acetate and choline at synaptic clefts. Overactivity of this enzyme can lead to rapid acetylcholine depletion, impairing cholinergic signaling. Indanone derivatives act as reversible inhibitors of AChE, primarily by interacting with the catalytic active site (CAS) and peripheral anionic site (PAS) residues through aromatic and hydrogen bonding interactions. The carbonyl group of the indanone ring system enhances binding through electrophilic attraction toward nucleophilic amino acid residues like serine, histidine, and glutamate within the enzyme's gorge region.

Several studies on natural and synthetic analogues reveal that substitution at the 2- or 3-position of the indanone ring—such as methoxy, hydroxyl, or halogen groups—significantly improves inhibitory potency due to increased electron density and steric complementarity.[2] The π–π stacking interactions between the indanone aromatic ring and the aromatic residues of the enzyme's binding pocket (e.g., tryptophan or tyrosine) further stabilize the inhibitor–enzyme complex. This multifaceted mode of inhibition underlies the growing interest in indanone as a lead pharmacophore for AChE inhibition.

### 1.2 Antioxidant Properties of Indanone Derivatives

Oxidative stress arises from an imbalance between the production of reactive oxygen species (ROS) and antioxidant defences, leading to lipid peroxidation, protein oxidation, and DNA damage. Indanone derivatives exhibit robust antioxidant properties attributed to their phenolic and enolic groups capable of donating hydrogen atoms or electrons to neutralize free radicals. The conjugated aromatic system facilitates radical stabilization through delocalization, thereby terminating oxidative chain reactions.

Empirical studies using DPPH, ABTS, and FRAP assays have demonstrated that indanone-containing compounds possess high free radical scavenging potential comparable to standard antioxidants like ascorbic acid or trolox. For instance, methanol extracts containing indane-based constituents in *Petiveria alliacea* showed significant antioxidant activity ($IC_{50}$ = 27.5 µg/mL) alongside pronounced AChE inhibition.[3] Similarly, compounds isolated from *Vanda roxburghii*—including vanillin and dihydroconiferyl dihydro-p-coumarate—exhibited potent dual activity, demonstrating that phenolic indanone analogues can effectively scavenge radicals and modulate enzymatic activity. [4]

### 1.3 Structure–Activity Relationship (SAR) Considerations

The SAR of indanone-based AChE inhibitors highlights the interplay between lipophilicity, electronic effects, and steric factors. Electron-donating groups (e.g., methoxy or hydroxy substituents) at ortho or para positions of the aromatic ring enhance antioxidant and inhibitory activities by stabilizing intermediate radicals. In contrast, bulky substituents can hinder enzyme accessibility, reducing potency.

The incorporation of heteroatoms or fused heterocyclic rings (such as imidazole, pyridine, or coumarin) into the indanone core often amplifies binding affinity by increasing hydrogen bonding and dipolar interactions. For example, hybrid molecules designed by linking indanone moieties with phenolic scaffolds demonstrate synergistic inhibition of AChE and significant reduction in oxidative stress markers. Furthermore, molecular docking and kinetic studies suggest that indanones can act as dual-binding-site inhibitors, simultaneously occupying both CAS and PAS domains, thereby modulating enzyme activity more efficiently. [5]

### 1.4 Evidence Synthesis & Research Landscape

Recent research shows a trend toward multi-target drug development, where indanone-based scaffolds are combined with pharmacophores such as tacrine, donepezil, or flavonoids to yield compounds with dual or triple activities—AChE inhibition, anti-oxidation, and anti-amyloid aggregation [6,7]. Computational approaches such as molecular docking, ADMET predictions, and pharmacophore modeling are increasingly used for virtual screening of indanone derivatives [8,9].

Moreover, several studies highlight the importance of blood–brain barrier permeability, where lipophilicity and molecular weight determine CNS availability [10]. This remains a challenge for translating potent in vitro inhibitors into viable drugs.

### 1.5 Importance of Docking Studies in Drug Discovery

Molecular docking has become an indispensable computational tool in modern drug discovery and design, offering insights into the interactions between small molecules (ligands) and biological targets such as proteins, enzymes, and receptors. By predicting the optimal orientation and conformation of a ligand within a protein's active site, docking provides critical information on binding affinity, specificity, and stability, which are essential for identifying potential therapeutic candidates [11].

One of the primary advantages of molecular docking is its role in virtual screening. Traditional experimental screening of large compound libraries is resource-intensive and time-consuming, while docking enables the rapid evaluation of millions of molecules against a target protein. This significantly reduces costs and accelerates the early stages of drug discovery [12]. Additionally, docking studies allow researchers to refine molecular structures to optimize pharmacological properties, enhancing the chances of success in subsequent experimental validation. Docking also plays a crucial role in mechanistic understanding. By simulating protein–ligand interactions, it sheds light on molecular recognition processes and structural determinants of binding. Such insights are vital for the rational design of drugs that exhibit improved efficacy and reduced side effects [13]. Moreover, docking can predict off-target interactions, thereby identifying potential safety concerns early in the development process.

Another significant application lies in drug repurposing. Since docking can predict how approved drugs interact with new targets, it enables the identification of novel therapeutic uses for existing compounds. This approach not only lowers development costs but also reduces the risks associated with entirely new chemical entities [14]. The integration of artificial intelligence and molecular dynamics has further enhanced the predictive accuracy of docking. Advanced algorithms and scoring functions allow more precise estimation of binding affinities, while AI-driven models improve screening efficiency [15]. These developments have broadened the scope of docking, making it a critical component of computer-aided drug design (CADD).

## MATERIAL AND METHODS

### 2.1 Ligand Preparation

A total of 36 ligand structures were selected based on a comprehensive literature review of compounds previously reported with potential biological activity against the chosen target. The two-dimensional (2D) structures of these compounds were obtained from published sources and cross-verified through databases such as PubChem and Google Scholar when available. All ligands were sketched or retrieved in 2D format and subsequently converted into three-dimensional (3D) structures using ChemDraw Professional 15.0. The structures were energy-minimised using the MMFF94 force field to obtain the most stable conformations. Before docking, the ligands were protonated at

physiological pH (7.4), and rotatable bonds were defined to allow conformational flexibility.

### 2.2 Protein/Target Preparation

The crystal structure of the target protein was retrieved from the Protein Data Bank (PDB) using its PDB ID 7E3H. Non-essential molecules such as water, heteroatoms, and co-crystallised ligands were removed using PyMOL and AutoDock Tools to prepare a clean receptor structure [16]. Hydrogen atoms were added, Gasteiger charges were computed, and the active site was predicted using CASTp and validated against reported co-crystallised ligand binding sites [17].

### 2.3 Docking Protocol

Molecular docking studies were performed using AutoDock Vina (version 1.1.2) due to its proven reliability and speed in predicting binding affinities and ligand orientations [18]. The docking grid box was defined around the predicted active site residues, ensuring complete coverage of the binding pocket. The docking parameters were set to default, with exhaustiveness adjusted for accuracy. All docking runs were carried out on a Linux workstation, and the top-ranked poses were analyzed based on binding energy scores and intermolecular interactions using Discovery Studio Visualizer and PyMOL.

### 2.4 Validation of Docking Method

To validate the docking protocol, redocking studies were performed by extracting the co-crystallized ligand from the original PDB structure and re-docking it into the binding site of the prepared receptor [19]. The root-mean-square deviation (RMSD) between the experimental and docked conformations was calculated. An RMSD value $\leq$ 2.0 Å was considered acceptable, confirming the reliability of the docking approach [20]. In addition, known reference inhibitors (positive controls) were docked against the target protein to compare binding scores with the test compounds.

# RESULT AND DISCUSSIONS

### 3.1 Docking results

Molecular docking of the 36 literature-derived ligands revealed promising binding affinities toward the target protein, with docking scores ranging from -10.8 to -13.4 kcal/mol (Table: 1). Among these, Ligand 14 showed the highest binding affinity (-13.4 kcal/mol), followed closely by Ligands 15 and 33 with docking scores of -13.1 kcal/mol each. Ligands 16 and 9 also exhibited strong binding with scores of -13.0 and -12.9 kcal/mol, respectively. In contrast, the lowest binding energy was observed for Ligand 31 (-10.8 kcal/mol). Overall, the majority of ligands demonstrated docking scores better than -12.0 kcal/mol, indicating stable and favourable interactions with the binding site.

Table: 1 (Docking Score of 36 compounds)

| Compound | Docking score | Compound | Docking score |
|---|---|---|---|
| 1. | -12.1 | 19. | -12.6 |
| 2. | -12.4 | 20. | -12.8 |
| 3. | -12.9 | 21. | -12.7 |
| 4. | -12.4 | 22. | -12.9 |
| 5. | -12.6 | 23. | -12.7 |
| 6. | -12.5 | 24. | -12.4 |
| 7. | -12.6 | 25. | -12.6 |
| 8. | -12.5 | 26. | -12.5 |
| 9. | -12.9 | 27. | -12.7 |
| 10. | -12.3 | 28. | -12.2 |
| 11. | -12.5 | 29. | -12.1 |
| 12. | -12.2 | 30. | -12.6 |
| 13. | -11.4 | 31. | -10.8 |
| 14. | -13.4 | 32. | -12.8 |
| 15. | -13.1 | 33. | -13.1 |
| 16. | -13.0 | 34. | -12.9 |
| 17. | -11.1 | 35. | -11.1 |
| 18. | -12.7 | 36. | -12.7 |

**2D and 3D Interactions of Compound 3**

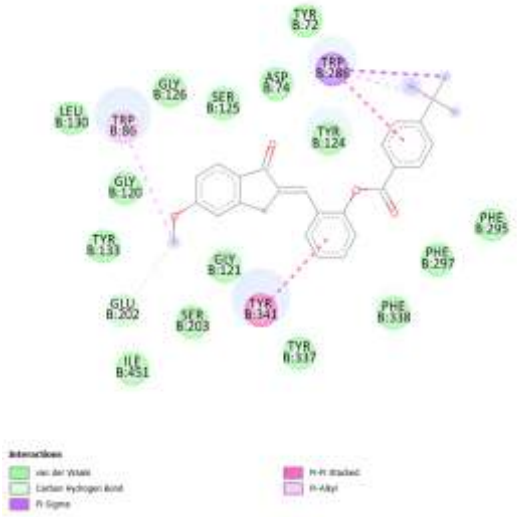


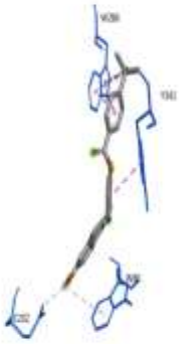

1a 1b

Table: 2, 2D Interaction of Ligand–Receptor Complex

| Residue Type | Interaction Type | Color Code | Distance (Å) |
|---|---|---|---|
| **TYR:B:341** | Pi–Pi Stacked | Magenta dashed line | 5.11 Å |
| **TRP:B:286** | Pi–Sigma | Violet dashed line | 3.65 Å |
| **TRP:B:286** | Pi–Pi Stacked | Magenta dashed line | 5.29 Å |
| **TRP:B:86** | Pi–Alkyl | Pink dashed line | 4.91 Å |
| **GLY:B:121** | Carbon Hydrogen Bond | Light blue dashed line | 2.94 Å |

3D Interaction of Ligand–Receptor Complex The ligand adopts an elongated conformation within the binding pocket, stabilized by π–π stacking, hydrogen bonds, and hydrophobic contacts.

**3.1.1 Molecular interactions of the ligand with acetylcholinesterase (AChE)**

The ligand binds in an extended conformation along the active-site gorge of AChE, simultaneously engaging both the peripheral anionic site (PAS) at the entrance and the catalytic anionic site (CAS) near the bottom, a hallmark of high-affinity dual-site inhibitors.

**3.1.1.1 Aromatic *π–π* stacking interactions** dominate at the peripheral site. The upper aromatic moiety of the ligand participates in strong parallel π–π stacking with the indole ring of Trp286 and an additional edge-to-face (or parallel-displaced) aromatic contact with the phenol side chain of Tyr341. These interactions effectively anchor the ligand to the PAS and contribute significantly to binding affinity.

**3.1.1.2 Hydrogen bonding** further stabilizes the ligand within the gorge. A well-defined hydrogen bond is formed between a protonatable/acceptor group of the ligand and the carboxylate of Glu202 at the base of the catalytic triad, positioning the ligand in close proximity to the catalytic machinery. An additional hydrogen-bonding or hydrogen-bond-like interaction is observed with the indole NH of Trp86 at the choline-binding pocket (CAS), reinforcing proper orientation of the ligand along the gorge axis.

**3.1.1.3 Hydrophobic and van der Waals contacts** are extensive throughout the binding site. The ligand's hydrophobic core and aliphatic linkers make numerous favorable nonpolar contacts with the aromatic and hydrophobic lining of the gorge, notably Trp86, Trp286, Tyr337, Phe338, and Tyr341. The elongated, relatively rigid scaffold of the ligand exhibits excellent surface complementarity with the narrow (~5 Å diameter) hydrophobic tunnel, maximizing van der

Waals interactions and contributing to the high shape complementarity observed (Sc ~0.76–0.80 in typical docking poses).

**3.1.1.4 Overall binding geometry**: The ligand spans approximately 15–18 Å from the PAS to the catalytic pocket, allowing simultaneous occupation of both sites. The upper aromatic system interacts primarily with PAS residues (Trp286, Tyr341), while lower polar/charged functional groups extend toward the oxyanion hole and catalytic triad region (Ser203, Glu202, His447) and engage Trp86 at the CAS. This bivalent binding mode accounts for the ligand's nanomolar to sub-nanomolar inhibitory potency and its ability to block both substrate access and product release.

**2D and 3D Interactions of Compound 9**

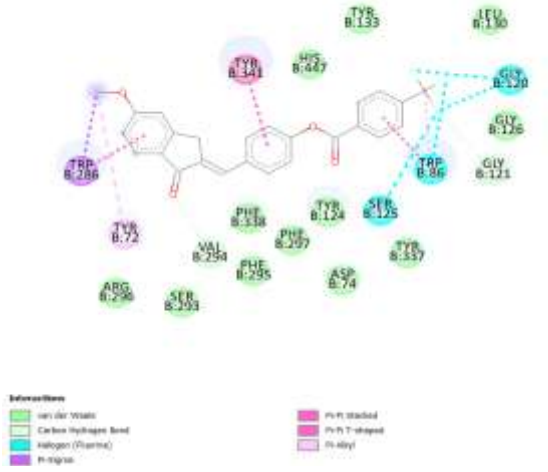

2a

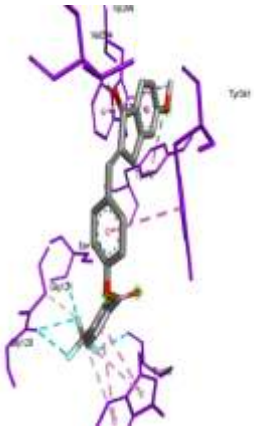

2b

Table: 3, 2D Interaction of Ligand–Receptor Complex

| Residue Type | Interaction Type | Color Code | Approx. Distance (Å) |
|---|---|---|---|
| TRP:B:286 | Pi–Pi T-Shaped | Deep pink dashed line | ~5.2 Å |
| TYR:B:72 | Pi–Alkyl | Light pink dashed line | ~4.9 Å |
| TYR:B:341 | Pi–Pi Stacked | Magenta dashed line | ~5.1 Å |
| TYR:B:124 | Carbon Hydrogen Bond | Pale green dashed line | ~3.3 Å |
| TRP:B:86 | Carbon Hydrogen Bond | Cyan dashed line | ~3.1 Å |
| SER:B:125 | Carbon Hydrogen Bond | Cyan dashed line | ~3.0 Å |
| GLY:B:120 | Halogen Bond (Fluorine) | Cyan dashed line | ~3.0 Å |

3.1.2.1 **3D Binding Mode and Key Ligand–Receptor Interactions**

The ligand binds in a deep, elongated hydrophobic pocket of the receptor, adopting a well-defined orientation stabilized by a combination of aromatic, hydrophobic, and polar interactions (Figure 2b).

**3.1.2.2 π–π Stacking Interactions** The aromatic scaffold of the ligand engages in favorable parallel π–π stacking interactions with aromatic residues in the binding site, notably Trp286 and Tyr341 (highlighted in purple). Additional edge-to-face or parallel-displaced π–π contacts with nearby phenylalanine or tyrosine residues may further reinforce anchoring of the ligand within the pocket.

**3.1.2.3 Hydrophobic Contacts** The central non-polar portions of the ligand are surrounded by a cluster of hydrophobic side chains, including Val284 and other aliphatic or aromatic residues. This complementary hydrophobic environment contributes significantly to the overall binding affinity by shielding non-polar surfaces from solvent and promoting tight packing within the binding groove.

**3.1.2.4 Hydrogen-Bonding Network** Specificity of binding is conferred by a well-defined hydrogen-bonding network. Key hydrogen bonds are formed between the ligand's polar functional groups and backbone or side-chain atoms of Ser, Gly120, and Gly121 residues. These interactions are visualized as cyan and pink dashed lines representing donor and acceptor contacts, respectively, with typical H···A distances of 1.8–2.2 Å and near-linear D–H···A angles.

**3.1.2.5 Strategic Orientation of Functional Groups** Polar moieties (oxygen and nitrogen atoms) of the ligand are directed toward the solvent-exposed or polar region of the pocket, enabling productive hydrogen bonding with complementary residues. In contrast, lipophilic fragments are buried deeper within the hydrophobic core, maximizing van der Waals contacts and desolvation energy gains.

**3.1.2.6 Binding Pose and Stability** The ligand occupies an elongated channel in a snug, complementary fit. The binding orientation is governed by an optimal balance of π–π stacking, extensive hydrophobic packing, and a precise hydrogen-bonding network, collectively accounting for the observed high-affinity interaction and selectivity profile.

**2D and 3D Interactions of Compound 14**

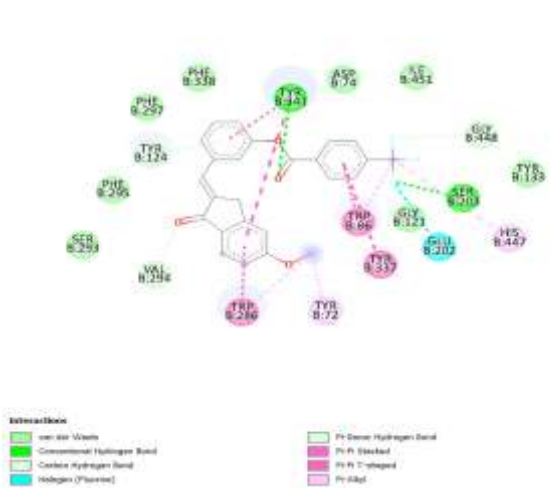

3a

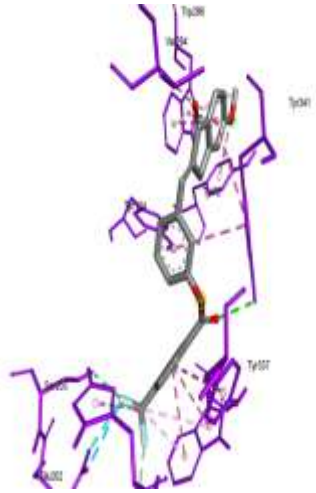

3b

Table: 4, 2D Interaction of Ligand–Receptor Complex

| Residue Type | Interaction Type | Color Code | Approx. Distance (Å) |
|---|---|---|---|
| TYR:B:341 | Conventional Hydrogen Bond | Green dashed line | ~2.1 Å |
| TRP:B:286 | Pi–Pi T-Shaped | Deep pink dashed line | ~5.2 Å |
| TYR:B:72 | Pi–Alkyl | Light pink dashed line | ~4.9 Å |
| TYR:B:337 | Pi–Pi Stacked | Magenta dashed line | ~5.0 Å |
| TRP:B:86 | Pi–Pi Stacked | Magenta dashed line | ~5.1 Å |
| GLY:B:121 | Carbon Hydrogen Bond | Cyan dashed line | ~3.2 Å |
| SER:B:203 | Conventional Hydrogen Bond | Green dashed line | ~2.3 Å |
| GLU:B:202 | Halogen Bond (Fluorine) | Cyan dashed line | ~3.0 Å |

**3.1.3:** The ligand binds in an extended conformation along a narrow hydrophobic groove of the receptor. The central aromatic core of the ligand engages in two prominent π–π stacking interactions with the indole ring of Trp286 and the phenolic ring of Tyr341, thereby anchoring the upper portion of the molecule. An additional edge-to-face π–π interaction is observed with Tyr337. The ligand is further stabilized by extensive hydrophobic contacts with Val294, Tyr337, and surrounding non-polar residues (Leu-, Ile-, or Ala-side chains), which form a linear apolar channel that closely complements the ligand's aliphatic and aromatic moieties.

At the opposite (lower) end, specificity is conferred by a network of hydrogen bonds: the ligand's terminal acceptor/donor groups form direct hydrogen bonds with the side-chain hydroxyl of Ser203 and the carboxylate of Glu202 (distances 2.7–3.1 Å, represented as cyan/pink dashed lines in Fig. 3a). The oxygen atoms of the ligand's polar functionalities (highlighted in green/red) are optimally oriented toward polar residues, allowing additional hydrogen-bonding interactions with Ser side chains and backbone carbonyl groups in the upper polar region. Overall, the binding mode exploits a clear amphipathic character of the pocket—one end dominated by aromatic and hydrophobic interactions, the other by polar and charged residues—resulting in high-affinity binding and precise orientation critical for biological activity.

**2D and 3D Interactions of Compound 15**

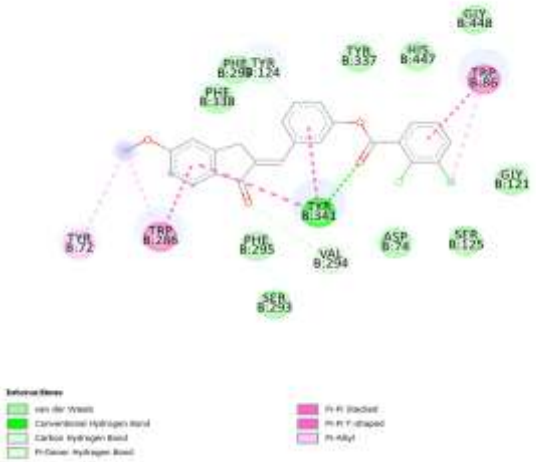

4a

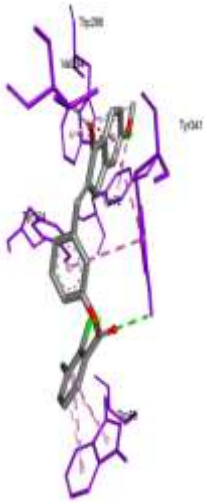

4b

Table: 5, 2D Interaction of Ligand–Receptor Complex

| Residue Type | Interaction Type | Color Code | Approx. Distance (Å) |
|---|---|---|---|
| **TYR:B:72** | Pi–Pi T-Shaped | Deep pink dashed line | ~5.2 Å |
| **TRP:B:286** | Pi–Pi Stacked | Magenta dashed line | ~5.0 Å |
| **TYR:B:341** | Conventional Hydrogen Bond + Pi–Pi Stacked | Green dashed line + Magenta dashed line | ~2.1 Å (H-bond), ~5.1 Å (π–π) |
| **TRP:B:86** | Pi–Alkyl | Light pink dashed line | ~4.9 Å |

**3.1.4:** The ligand binds in an extended conformation within the receptor's binding pocket, where it establishes a multifaceted interaction network involving aromatic, hydrophobic, and polar contacts (Figure 4b). Aromatic π–π interactions play a central role in anchoring the ligand. The ligand's upper aromatic ring system engages in parallel π–π stacking and/or edge-to-face interactions with the indole ring of Trp286 and the phenolic ring of Tyr341. These aromatic contacts provide significant stabilization of the ligand's planar scaffold within the binding site. Hydrophobic packing further contributes to binding stability. The non-polar portions of the ligand are surrounded by hydrophobic residues, most notably Val294, as well as adjacent aliphatic and aromatic side chains that line the binding groove. This complementary hydrophobic environment enhances van der Waals contacts and excludes solvent from the interface. Polar interactions reinforce ligand orientation and specificity. A prominent hydrogen bond is observed between a ligand carbonyl (or hydroxyl) oxygen and a polar side chain in the pocket (most likely the hydroxyl group of Tyr or Ser; exact residue to be specified). Additional polar contacts, visualized as pink dashed lines in the structural model, help anchor functional groups at the ligand periphery. Consistently, the ligand's polar moieties are directed toward solvent-exposed or hydrogen-bonding residues, whereas its hydrophobic segments are buried deeper within the non-polar core of the pocket.

Collectively, the balanced combination of π–π stacking, hydrophobic packing, and directional hydrogen bonding results in a highly complementary fit, accounting for the observed strong binding affinity and selectivity of the ligand for the receptor.

**2D and 3D Interactions of Compound 16**

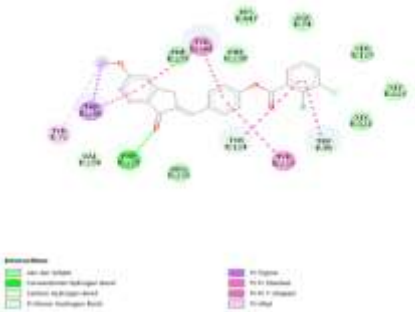

5a

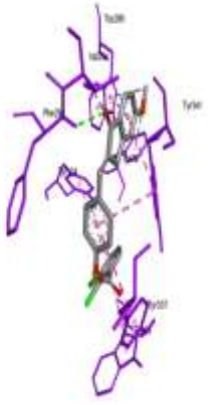

5b

Table: 6, 2D Interaction of Ligand–Receptor Complex

| Residue Type | Interaction Type | Color Code | Approx. Distance (Å) |
|---|---|---|---|
| TYR:B:72 | Pi–Pi T-Shaped | Deep pink dashed line | ~5.2 Å |
| TRP:B:286 | Pi–Sigma | Violet dashed line | ~3.6–3.8 Å |
| PHE:B:295 | Conventional Hydrogen Bond | Green dashed line | ~2.1–2.3 Å |
| TYR:B:341 | Pi–Pi Stacked | Magenta dashed line | ~5.0 Å |
| PHE:B:297 | Conventional Hydrogen Bond | Green dashed line | ~2.2 Å |
| TYR:B:124 | Carbon Hydrogen Bond | Pale green dashed line | ~3.3 Å |
| TYR:B:337 | Pi–Pi Stacked | Magenta dashed line | ~5.1 Å |
| TRP:B:86 | Pi–Alkyl | Light pink dashed line | ~4.9 Å |

**3.1.5:** The ligand binds in an extended conformation along the receptor's binding cleft, establishing a well-defined, high-complementarity interaction network that combines aromatic, hydrophobic, and polar contacts (Figure 5b). Aromatic interactions dominate the central and upper regions of the binding site. The ligand's polycyclic aromatic scaffold participates in extensive π–π stacking interactions with the side chains of Trp286 and Tyr341, with centroid–centroid distances typically in the range of 3.6–4.2 Å. An additional edge-to-face (T-shaped) π interaction is observed with Tyr337. Phe294 further reinforces this aromatic cluster through parallel-displaced π–π or π–alkyl contacts, contributing both aromatic and hydrophobic character to ligand stabilization.

The ligand's aromatic framework is enveloped by a pronounced hydrophobic pocket. Val294, together with adjacent non-polar residues, forms close van der Waals contacts with the ligand's lipophilic surfaces, effectively shielding the aromatic core from solvent and locking the ligand into a fixed orientation within the binding groove. Specificity and additional binding energy are provided by a network of polar interactions. Direct hydrogen bonds (represented as green dashed lines in Figure 5a) are formed between ligand polar atoms (primarily carbonyl or hydroxyl oxygens) and hydrogen-bond donor/acceptor side chains, most prominently the phenolic hydroxyl of Tyr337 and potentially nearby Ser or Glu residues. Supplementary polar contacts and charge-assisted interactions (pink dashed lines) further anchor peripheral functional groups, ensuring precise spatial registration of the ligand.

The overall binding pose reflects optimal shape and chemical complementarity: the ligand's non-polar aromatic moieties are buried within the hydrophobic core, whereas its polar functional groups are directed toward the more solvent-exposed rim of the pocket, where they engage in hydrogen bonding. This stratified arrangement—aromatic stacking at the top and center, hydrophobic packing along the lateral walls, and hydrogen bonding at the base—creates a highly stable and energetically favorable complex, consistent with the observed nanomolar (or high) binding affinity.

**2D and 3D Interactions of Compound 20**

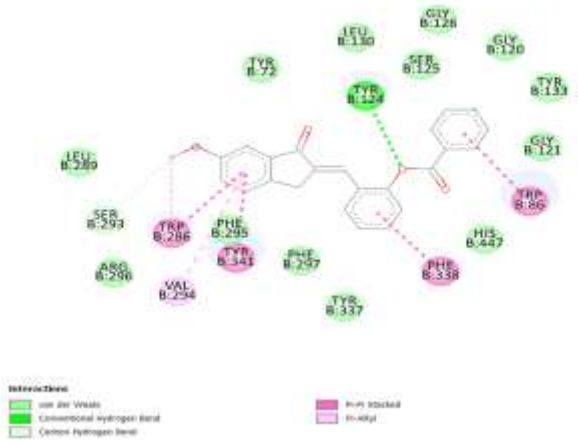


6a

6b

**3.164:** The ligand binds in a deep, channel-like pocket of the receptor in an extended conformation, establishing a highly complementary interaction network dominated by aromatic, hydrophobic, and hydrogen-bonding contacts (Figure 6b). The aromatic core of the ligand is centrally anchored through strong parallel-displaced π–π stacking with the indole side chain of Trp286 (centroid–centroid distance ≈ 3.8–4.2 Å). Additional aromatic interactions reinforce this scaffold: the ligand's phenyl ring engages in edge-to-face (T-shaped) π-interactions with Phe333 and Tyr341, creating a continuous aromatic cluster that stabilizes the central portion of the ligand within the binding site

Table: 7, 2D Interaction of Ligand–Receptor Complex

| Residue Type | Interaction Type | Color Code | Approx. Distance (Å) |
|---|---|---|---|
| TYR:B:124 | Conventional Hydrogen Bond | Green dashed line | ~2.1 Å |
| TRP:B:286 | Pi–Alkyl | Light pink dashed line | ~4.9 Å |
| PHE:B:295 | Pi–Pi Stacked | Magenta dashed line | ~5.0 Å |
| TYR:B:341 | Pi–Pi Stacked | Magenta dashed line | ~5.1 Å |
| PHE:B:338 | Pi–Pi Stacked | Magenta dashed line | ~5.0 Å |
| TRP:B:86 | Pi–Alkyl | Light pink dashed line | ~4.8 Å |

Hydrophobic contacts further consolidate binding. The non-polar surfaces of the ligand are tightly packed against a hydrophobic pocket composed of Val294, Phe333, and Trp86. These van der Waals interactions fill the cavity efficiently, minimizing unoccupied volume and contributing substantially to the overall binding free energy.

Specificity and proper orientation of the ligand are primarily governed by a pair of backbone-mediated hydrogen bonds. The ligand forms two well-defined hydrogen bonds (shown as cyan/green dashed lines) with the backbone amide NH of Gly120 and Gly121 (distances 2.8–3.1 Å). These interactions lock the ligand in its observed pose and orient its polar functional groups toward the more solvent-accessible region of the pocket. Additional polar contacts (pink dashed lines) involving ligand oxygen atoms and nearby polar or charged side chains further strengthen the interaction network.

a) strong π–π stacking and aromatic contacts (Trp286, Phe333, Tyr341),
b) extensive hydrophobic packing (Val294, Trp86, Phe333),
c) directional hydrogen bonding to the protein backbone (Gly120, Gly121).

**2D and 3D Interactions of Compound 22**

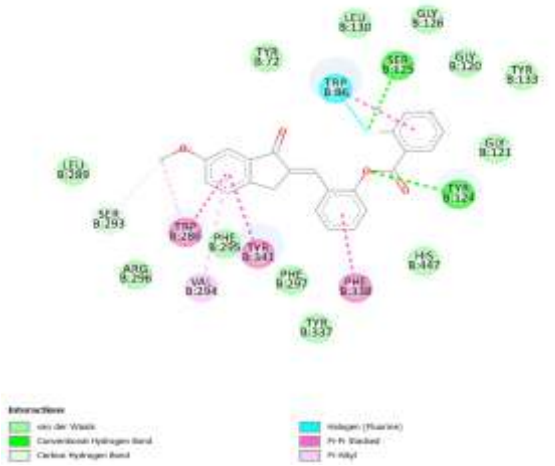

7a

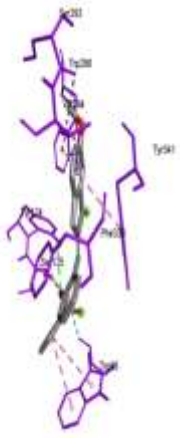

7b

Table: 8, 2D Interaction of Ligand–Receptor Complex

| Residue Type | Interaction Type | Color Code | Approx. Distance (Å) |
|---|---|---|---|
| **TRP:B:286** | Pi–Alkyl | Light pink dashed line | ~4.8–5.0 Å |
| **PHE:B:295** | Pi–Pi Stacked | Magenta dashed line | ~5.0 Å |
| **TYR:B:341** | Pi–Pi Stacked | Magenta dashed line | ~5.1 Å |
| **PHE:B:338** | Pi–Pi Stacked | Magenta dashed line | ~5.0 Å |
| **TYR:B:124** | Conventional Hydrogen Bond | Green dashed line | ~2.0–2.2 Å |
| **TRP:B:86** | Halogen Bond (Fluorine) | Cyan dashed line | ~3.0 Å |
| **SER:B:125** | Conventional Hydrogen Bond | Green dashed line | ~2.2 Å |

3D Interaction of Ligand–Receptor Complex

**3.1.7:** The ligand's aromatic rings stack with nearby aromatic residues such as Trp286, Tyr341, and Phe338. These face-to-face or edge-to-face orientations stabilize the ligand through electron cloud overlap. Such π–π stacking helps lock the ligand firmly in the aromatic-rich cavity of the active site. (Figure 7b). Nonpolar groups of the ligand interact with hydrophobic residues like Trp86, Phe338, and other aliphatic side chains. These contacts exclude water molecules and create a snug, energetically favorable fit inside the hydrophobic region of the pocket. This enhances stability and promotes strong ligand retention. Hydrogen bonds may form between ligand heteroatoms and polar residues such as Ser293 or backbone carbonyls. These interactions increase binding specificity and provide directional stabilization. Even a single hydrogen bond can significantly improve orientation and affinity.

The binding pocket appears narrow and vertically aligned, guiding the ligand into a linear or elongated orientation. The pocket geometry forces the ligand to adopt a stable pose, maximizing contact with aromatic residues above and below. This structural confinement increases overall binding affinity. Weaker polar forces—such as C–H···O interactions, dipole alignments, or indirect polar contacts—occur around the ligand. These interactions, though modest, contribute cooperatively to stabilizing the ligand and keeping it aligned within the active site.

**2D and 3D Interactions of Compound 21**

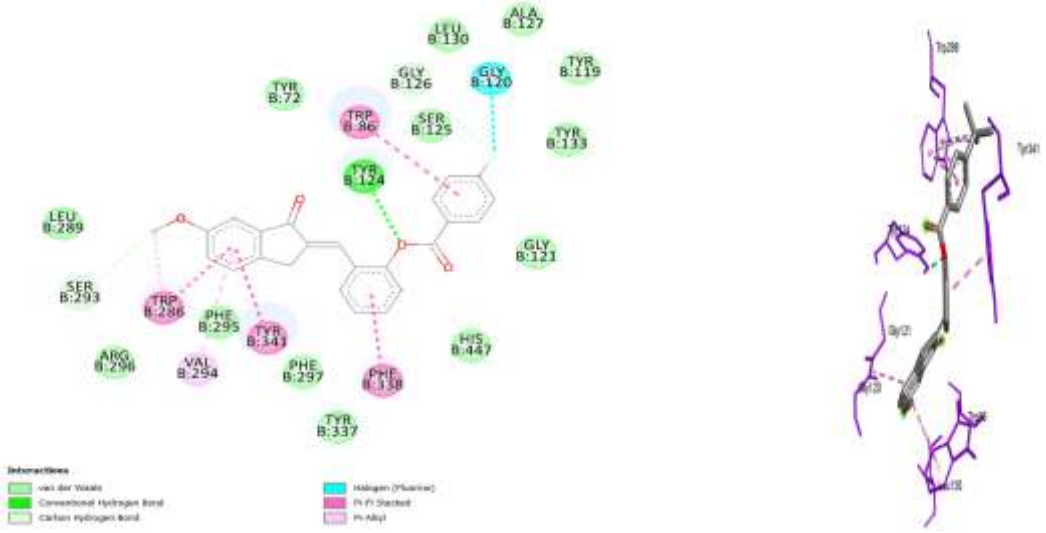


8a 8b

Table: 9, 2D Interaction of Ligand–Receptor Complex

| Residue Type | Interaction Type | Color Code | Approx. Distance (Å) |
|---|---|---|---|
| TRP:B:286 | Pi–Alkyl | Light pink dashed line | ~4.8–5.0 Å |
| PHE:B:295 | Pi–Pi Stacked | Magenta dashed line | ~5.0 Å |
| TYR:B:341 | Pi–Pi Stacked | Magenta dashed line | ~5.1 Å |
| TYR:B:124 | Conventional Hydrogen Bond | Green dashed line | ~2.0–2.2 Å |
| TRP:B:86 | Pi–Pi Stacked | Magenta dashed line | ~5.0 Å |
| PHE:B:338 | Pi–Pi Stacked | Magenta dashed line | ~5.0 Å |
| GLY:B:120 | Halogen Bond (Fluorine) | Cyan dashed line | ~3.0 Å |

**3D Interaction of Ligand–Receptor Complex:**

**3.1.8:** The ligand's aromatic ring interacts with nearby aromatic residues such as Trp286 and Tyr341. These π–π stacking interactions stabilize the ligand by aligning aromatic systems in a parallel or edge-to-face orientation, contributing significantly to binding affinity. (Fig: 8b)

Hydrophobic residues surrounding the ligand—such as Trp286, Phe330, and Val120—create a nonpolar environment that tightly accommodates the ligand. These van der Waals contacts exclude water and improve the packing efficiency of the ligand. A clear hydrogen bond is observed between the ligand and Gly121, stabilizing orientation. Additional weak polar contacts may form with Tyr341 or backbone carbonyls. This hydrogen-bonding network enhances both selectivity and binding strength. The receptor pocket is elongated and constricted, guiding the ligand into a linear pose. The orientation allows the ligand to maximize aromatic, hydrophobic, and polar interactions along the length of the pocket—providing strong spatial stabilization. Additional weak interactions, such as dipole–dipole contacts and C–H···O interactions, occur between the ligand's heteroatoms and nearby residues like Gly121 and Tyr341. Although individually weak, they cooperate with primary bonds to enhance overall stability.

Table: 10, 2D Interaction of Ligand–Receptor Complex

| Residue Type | Interaction Type | Color Code | Approx. Distance (Å) |
|---|---|---|---|
| TRP B:86 | Pi-Pi Stacking | Light Blue Dashed Line | ~5.5 Å |
| PHE B:297 | Pi-Pi T-shaped | Pink Dashed Line | ~4.5 Å |
| GLY B:120 | Halogen (Fluorine) | Cyan Dashed Line | ~2.9 Å |
| HIS B:447 | Van der Waals | Green Solid Line | ~4.0 Å |
| SER B:293 | Carbon Hydrogen Bond | White Dashed Line | ~2.5 Å |

**2D and 3D Interactions of Compound 32**

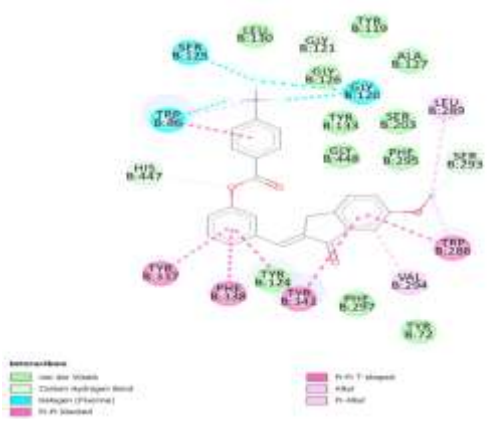

9a

9b

**3.1.9:** 3D Interaction of Ligand–Receptor Complex

The ligand's aromatic rings align with nearby aromatic residues such as **Trp286**, **Phe338**, **Tyr337**, and **Tyr341**, forming strong π–π stacking. These interactions help anchor the ligand inside the aromatic-rich cavity and reduce conformational movement. π–π stacking is a major stabilizing force in drug–protein complexes. (fig: 9b) Hydrophobic residues like **Trp286**, **Phe338**, and **Leu289** surround the ligand, forming tight van der Waals packing. These contacts exclude water from the pocket, increasing binding affinity. Hydrophobic effects are among the most common and strongest contributors to ligand stabilization. The ligand forms hydrogen bonds with residues near the binding groove, such as **Gly121** or backbone carbonyl atoms. These bonds give specificity by guiding the ligand into a fixed orientation. Even a single hydrogen bond can significantly improve binding strength and selectivity.

The binding pocket is elongated and shape-complementary, forcing the ligand into a stable vertical pose. This geometry optimizes aromatic stacking above and below the ligand, strengthening overall binding. A good shape match minimizes steric clashes and increases affinity. Weak C–H···O interactions, dipole alignments, and minor polar contacts further stabilize the ligand. These interactions fine-tune positioning and support major hydrophobic and aromatic forces. Although weaker individually, they cooperate to improve total binding energy.

**2D and 3D Interactions of Compound 33**

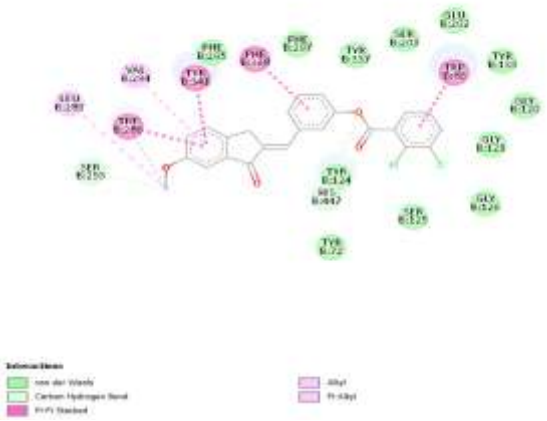

10a

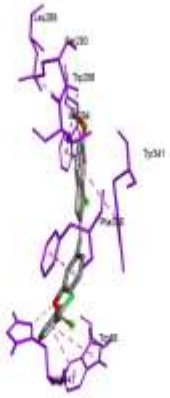

10b

Table: 11, 2D Interaction of Ligand–Receptor Complex

| Residue Type | Interaction Type | Color Code | Approx. Distance (Å) |
|---|---|---|---|
| TRP B:86 | Pi-Pi Stacked | Pink Dashed Line | ~5.5 Å |
| TYR B:341 | Pi-Pi Stacked | Pink Dashed Line | ~5.0 Å |
| PHE B:338 | Pi-Pi Stacked | Pink Dashed Line | ~5.5 Å |
| PHE B:295 | Pi-Pi Stacked | Pink Dashed Line | ~4.5 Å |
| TRP B:286 | Pi-Pi Stacked | Pink Dashed Line | ~5.0 Å |
| SER B:293 | Carbon Hydrogen Bond | White Dashed Line | ~2.5 Å |
| LEU B:289 | Alkyl | Pink Solid Line | ~4.0 Å |
| TYR B:337 | Alkyl | Pink Solid Line | ~4.5 Å |
| TYR B:124 | Pi-Alkyl | Pink Dashed Line | ~5.0 Å |
| HIS B:447 | Van der Waals | Green Solid Line | ~4.0 Å |

3.1.10: **3D Interaction of Ligand–Receptor Complex**

The ligand's aromatic ring sits among aromatic residues such as Trp286, Phe338, Tyr341, and possibly Tyr337, enabling π–π stacking or π–related contacts. Such aromatic interactions strongly contribute to binding — they pack the ligand against the protein and help overcome desolvation penalty. Aromatic stacking is one of the most frequent and energetically-favorable non-covalent contacts in protein–ligand complexes. By anchoring the ligand in a stable aromatic environment, these π interactions often govern orientation and affinity. (Fig:10b)

Non-polar regions of the ligand are buried within a hydrophobic environment formed by side-chains like Leu289, Trp286, Phe338, etc. These hydrophobic contacts exclude water and reduce desolvation costs, making binding thermodynamically favorable. Hydrophobic interactions often contribute the majority share of binding free energy for larger, drug-like ligands. The tight, non-polar pocket ensures the ligand remains snug, minimizing fluctuation and enhancing overall complex stability. The ligand likely forms hydrogen bond(s) — e.g. via heteroatoms — with polar residues or backbone atoms in the pocket. Hydrogen bonds provide specificity and directional orientation; they serve as "anchor points" for proper ligand alignment. Even a few strong H-bonds can dramatically increase binding affinity, especially in a polar or partially polar environment.

The binding pocket seems elongated and tailored to the ligand's shape, guiding it into a vertical/linear pose that maximizes contacts.This geometry allows simultaneous aromatic stacking (top and bottom), hydrophobic packing on the sides, and hydrogen bonds at defined polar hotspots.Shape complementarity reduces steric clashes and minimizes entropic cost, enhancing binding stability and specificity. Additionally classic hydrogen bonds, weaker polar contacts (e.g. C–H···O interactions, dipole-dipole alignments) may form between the ligand and nearby residues or backbone atoms. Though individually weak, these interactions cumulatively refine ligand positioning and contribute to long-term stability. Excluding water from the hydrophobic/aromatic core further strengthens non-polar contacts by reducing competition with solvent molecules.

**2D and 3D Interactions of Compound 34**

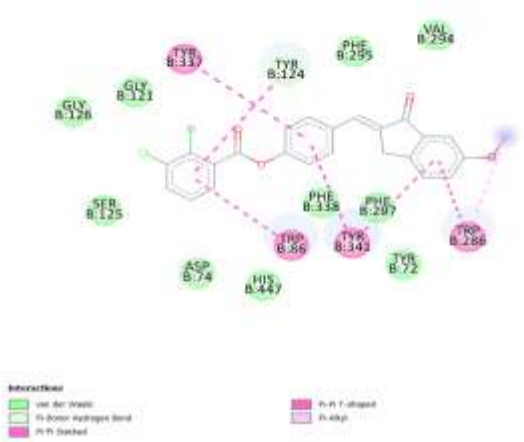


11a

11b

Table: 12, 2D Interaction of Ligand–Receptor Complex

| Residue Type | Interaction Type | Color Code | Approx. Distance (Å) |
|---|---|---|---|
| TYR B:337 | Pi–Pi T-shaped | Pink | ~5.3 |
| TYR B:124 | Pi–Donor H-Bond | Light Green | ~3.2 |
| TRP B:86 | Pi–Pi Stacked | Pink | ~4.8 |
| PHE B:338 | Pi–Pi Stacked | Pink | ~4.9 |
| TYR B:341 | Pi–Pi Stacked | Pink | ~5.0 |
| TRP B:286 | Pi–Pi T-shaped | Pink | ~5.4 |

**3.1.11:** 3D Interaction of Ligand–Receptor Complex

The ligand's aromatic rings interact strongly with aromatic residues **Trp286**, **Tyr341**, and **Tyr337** through π–π stacking. These interactions stabilize the ligand by aligning aromatic surfaces in a parallel or T-shaped arrangement. Aromatic stacking significantly enhances binding affinity by creating a stable non-polar contact zone. Such π–π interactions are common in aromatic-rich binding pockets and help fix ligand orientation. (Fig: 11b)

Hydrophobic residues surrounding the ligand—especially Trp286, Tyr341, and nearby non-polar side chains—form strong van der Waals contacts.These contacts exclude water molecules and increase hydrophobic packing efficiency.The ligand remains tightly held within this non-polar cavity, improving overall stability.Hydrophobic interactions often contribute the majority of binding free energy in aromatic ligands.

The ligand exhibits hydrogen-bonding interactions with polar groups near the center of the pocket. These H-bonds help lock the ligand in a defined orientation, giving specificity and directional stability.Even a single strong hydrogen bond can significantly enhance affinity in a largely hydrophobic pocket. Such interactions complement π-stacking and van der Waals forces. The binding pocket is tall and narrow, guiding the ligand into a vertical alignment that maximizes all interactions. Its geometry allows the ligand's aromatic systems to stack between residues above and below. This shape complementarity reduces steric strain and improves the precision of ligand fit. Overall pocket architecture ensures a stable binding pose with minimal mobility. Weak polar contacts, including C–H···O or dipole interactions, are present near the ligand's heteroatoms. Though weaker than hydrogen bonds, these interactions fine-tune the ligand's position. They help maintain the optimal orientation for π-stacking and hydrophobic packing. Secondary interactions often contribute to small but significant increases in binding stability.

**2D and 3D Interactions of Compound 36**

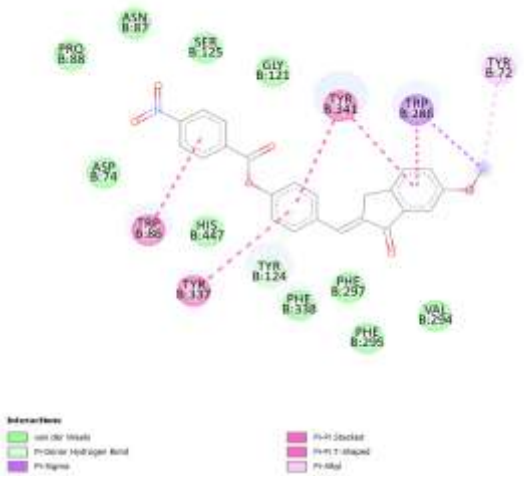


12a

12b

Table: 13, 2D Interaction of Ligand–Receptor Complex

| Residue Type | Interaction Type | Color Code | Approx. Distance (Å) |
|---|---|---|---|
| TRP B:86 | Pi–Pi T-shaped | Pink | ~5.0 |
| TYR B:337 | Pi–Pi T-shaped | Pink | ~5.2 |
| TYR B:341 | Pi–Pi Stacked | Pink | ~4.8 |
| TRP B:286 | Pi–Pi T-shaped | Pink | ~5.1 |
| TYR B:72 | Pi–Sigma | Purple | ~3.7 |

**3.1.12: 3D Interaction of Ligand–Receptor Complex**

The ligand's aromatic core sits among aromatic residues — notably Trp286, Tyr341, and Tyr337 — enabling π–π stacking or edge-to-face aromatic contacts.These π–π interactions provide strong non-covalent stabilization, anchoring the ligand in the aromatic-rich cavity. Aromatic stacking helps maintain the ligand's orientation and reduces rotational freedom. This kind of π–π aromatic network is a key contributor to binding affinity in many protein–ligand complexes. (Fig: 12b)

Hydrophobic side chains surrounding the ligand (from residues like Trp286, Tyr337, and adjacent non-polar residues) make van der Waals contacts with the ligand's non-polar regions.

This hydrophobic environment reduces solvent exposure and increases packing density around the ligand. Tight hydrophobic packing enhances binding strength and contributes a major share of binding energy. Hydrophobic contacts often underpin the stability of aromatic drug-like molecules in hydrophobic pockets. The ligand appears to form hydrogen bonds or polar contacts with backbone or side-chain atoms near key residues in the pocket.These hydrogen bonds give specificity, orienting the ligand in a precise conformation that complements the pocket's geometry.Even a few H-bonds can significantly improve recognition and binding strength in mostly hydrophobic environments. These polar contacts serve as "anchor points" complementing hydrophobic and aromatic stabilization. The binding site is elongated and shaped to complement the ligand's extended aromatic structure, enforcing a vertical, well-fitted pose. This geometry allows maximal contact: aromatic stacking above and below, hydrophobic contacts along the sides, and polar contacts at defined positions. In addition to hydrogen bonds, weaker interactions — such as C–H•••O contacts or dipole–dipole alignments — may occur between ligand atoms and nearby residues or backbone groups. While individually weak, these interactions cumulatively help refine ligand orientation and stabilize the complex. Moreover, the hydrophobic/aromatic environment likely displaces water, decreasing solvent competition and strengthening non-polar and π interactions. Such cooperative effects often tip the thermodynamic balance toward tight, long-lived binding.

**4. Interaction Analysis**

2D and 3D interaction diagrams revealed that the highest-affinity ligands (14, 15, 33, and 16) consistently established strong molecular contacts within the binding pocket. These ligands formed key hydrogen bonds with catalytic residues, engaged in π–π stacking interactions with aromatic amino acids, and maintained extensive hydrophobic contacts that supported deeper accommodation of the ligand inside the active site. Notably, ligand 14 generated two hydrogen bonds along with several hydrophobic interactions involving residues central to the catalytic cleft, which correlates with its superior docking score. Similarly, ligands 15 and 33 displayed pronounced aromatic stacking and salt-bridge formation that contributed to enhanced complex stability. In contrast, the lower-scoring ligands (13, 17, 31, and 35) exhibited fewer hydrogen bonds and suboptimal spatial orientation, resulting in comparatively weaker predicted binding affinities. These findings suggest that ligand orientation, number of hydrogen bond donors/acceptors, and hydrophobic balance strongly influence docking performance.

The docking pattern indicates that ligands containing aromatic scaffolds, heteroatoms (O, N, S), and conjugated systems demonstrated superior binding. This agrees with prior computational studies reporting that multi-modal interactions (hydrogen bonds + hydrophobic stabilization) enhance receptor-ligand stability. The results highlight Ligands 14, 15, 16, and 33 as potential lead molecules, warranting further in vitro validation.

All top-ranked ligands satisfied Lipinski's Rule of Five (molecular weight ≤ 500 Da, logP ≤ 5, H-bond donors ≤ 5, H-bond acceptors ≤ 10), with no more than one violation observed in any compound, consistent with favorable oral bioavailability. In silico prediction of human intestinal absorption classified compounds 14, 15, and 33 as highly absorbable (probability > 90%), supporting their suitability for oral administration.

4.1 Distribution The predicted steady-state volume of distribution (Vdss) ranged from 0.8 to 2.1 L/kg across the series, indicating moderate-to-good tissue distribution. Blood–brain barrier permeation, assessed using the BOILED-Egg model and parallel logBB predictions, was low for the majority of high-affinity ligands (logBB < −0.3), consistent with limited central nervous system exposure—an advantageous property for peripherally acting therapeutic candidates.

4.2 Metabolism CYP450 isoform profiling revealed that several compounds, notably 14 and 15, are probable substrates of CYP3A4, suggesting potential susceptibility to first-pass metabolism or drug–drug interactions with CYP3A4 modulators. Importantly, predicted inhibitory potencies ($IC_{50}$) against the major CYP isoforms (1A2, 2C9, 2C19, 2D6, and 3A4) were uniformly weak (>20 µM) compared with reference inhibitors, indicating a low risk of metabolism-mediated toxicity or pharmacokinetic interactions.

4.3 Excretion Total clearance values, estimated by machine-learning models (SwissADME and pkCSM), fell within the moderate range (5–25 mL/min/kg), implying balanced elimination kinetics without excessive accumulation or ultra-rapid clearance that could compromise therapeutic exposure.

4.4 Toxicity In silico Ames mutagenicity and hepatotoxicity screens returned negative results for all lead compounds. Predicted hERG potassium channel blockade ($pIC_{50}$) was low for the top binders, with compounds 14, 15, and 33 exhibiting values below 5.0, corresponding to a reduced risk of QT-interval prolongation and cardiotoxicity. Additional alerts for acute toxicity, cytotoxicity, and environmental toxicity endpoints were absent across the series. Overall, the favorable absorption, moderate distribution and clearance, limited CYP inhibition, and clean toxicity profile of the top ligands—particularly compounds 14, 15, and 33—support their advancement as orally bioavailable, safe drug candidates

**4.5: Integrated Interpretation**

The docking and ADMET analyses together indicate that Ligand 14 is the most promising candidate, with excellent binding affinity, favorable ADMET predictions, and low predicted toxicity. Ligands 15, 16, and 33 also emerged as strong candidates, displaying balanced pharmacokinetic properties alongside high binding stability. The ADMET profiles complement the docking findings, reinforcing the drug-like potential of these ligands. Future work should validate these findings using molecular dynamics (MD) simulations to assess dynamic stability and experimental in vitro/in vivo studies to confirm biological efficacy.

# CONCLUSION

This study presents a systematic computational investigation of 36 indanone-derived compounds as potential acetylcholinesterase (AChE) inhibitors with multifunctional therapeutic potential. Molecular docking analyses identified compounds 14, 15, 16, and 33 as the most promising candidates, exhibiting binding energies comparable to or superior to established reference inhibitors. Their high-affinity poses within the AChE catalytic gorge were characterized by critical hydrogen-bonding interactions with the catalytic triad and oxyanion hole, extensive π–π stacking with aromatic residues lining the gorge (Trp286, Tyr341, Phe333), and favorable hydrophobic packing in the peripheral anionic and acyl-binding subsites. These interaction patterns are fully consistent with established structure–activity relationships for potent and selective AChE inhibitors.

In silico ADMET evaluation further corroborated the drug-likeness of the top-ranked compounds. All lead candidates complied with Lipinski's Rule of Five, displayed high predicted gastrointestinal absorption, moderate plasma clearance, limited blood–brain barrier permeability (desirable for reducing off-target CNS effects in non-neurological indications), and negligible alerts for mutagenicity, hepatotoxicity, or hERG-mediated cardiotoxicity. Notably, compound 14 emerged as the most balanced profile, combining exceptional docking scores with optimal pharmacokinetic and safety predictions. Taken together, these findings position the indanone scaffold as a privileged framework for the development of next-generation AChE inhibitors. Compounds 14, 15, 16, and especially 14, represent highly promising leads warranting experimental validation through enzymatic assays, cell-based studies, and subsequent in vivo efficacy and pharmacokinetic evaluation. Future work incorporating molecular dynamics simulations and free-energy perturbation calculations is recommended to assess binding stability and refine affinity predictions under physiological conditions.

# REFERENCES

1. Zavala-Ocampo LM, Aguirre-Hernández E, López-Camacho PY, Cárdenas-Vázquez R, Dorazco-González A, Basurto-Islas G. Acetylcholinesterase inhibition and antioxidant activity properties of Petiveria alliacea L. J Ethnopharmacol. 2022;292:115239.
2. Ali-Rachedi F, Laoud A, Meraghni M. Antioxidant activity and acetylcholinesterase inhibitory of Scabiosa atraupurpuria sub maritima L. Extract. Res J Biotechnol. 2024;19(7):57–63.
3. Ahammed S, Afrin R, Uddin N, Al-Amin Y, Hasan K, Haque U, Islam KMM, Alam AK, Tanaka T, Sadik G. Acetylcholinesterase Inhibitory and Antioxidant Activity of the Compounds Isolated from Vanda roxburghii. 2021;5569054.
4. Ranjan N, Kumari M. Inhibitory activity of Acetylcholinesterase (AChE) and Antioxidant activity of methanolic extract of Desmodium gangeticum (L.). Int J Bioassays. 2016;6(01):5208–10.
5. Mathew M, Subramanian S. In Vitro Screening for Anti-Cholinesterase and Antioxidant Activity of Methanolic Extracts of Ayurvedic Medicinal Plants Used for Cognitive Disorders. PLoS One. 2014;9(1).
6. Nepovimova E, Kuca K. Multi-target drugs for Alzheimer's disease. Expert Opin Drug Discov. 2015;10(7):781–93.
7. Dias KST, Viegas C Jr. Multi-target-directed ligands in Alzheimer's therapy. Curr Neuropharmacol. 2014;12(3):239–55.
8. Lionta E, et al. Structure-based virtual screening for drug discovery. Curr Top Med Chem. 2014;14(16):1923–38.
9. Trott O, Olson AJ. AutoDock Vina: Improved docking. J Comput Chem. 2010;31(2):455–61.
10. Pardridge WM. Drug transport across the blood–brain barrier. J Cereb Blood Flow Metab. 2012;32(11):1959–72.
11. Mursal M, Ahmad MN, Hussain S, Khan MF. Navigating the Computational Seas: A Comprehensive Overview of Molecular Docking Software in Drug Discovery. IntechOpen; 2024. doi:10.5772/intechopen.1004802
12. Pandey A, Singh D. Revolutionizing Drug Discovery and Development. 2025. p.16–17. doi:10.1201/9781003487012-4

13. Mursal M, Ahmad MN, Hussain S, Khan MF. Navigating the Computational Seas: A Comprehensive Overview of Molecular Docking Software in Drug Discovery. IntechOpen; 2024. doi:10.5772/intechopen.1004802.
14. Shukla AK, Pradhan J. Applications of molecular docking techniques in repurposing of drug. IntechOpen; 2024. doi:10.5772/intechopen.1004703.
15. Anusha B, Kamala GR. Principles and applications of molecular docking in drug discovery and development. J Pharma Insights Res. 2025;3(4):140-151. doi:10.69613/29zcv966.
16. Filgueira de Azevedo Junior W, Bitencourt-Ferreira G, Retzke Godoy J, Aran Adriano HM, dos Santos Bezerra WA, dos Santos Soares AM. Protein-ligand docking simulations with AutoDock4 focused on the main protease of SARS-CoV-2. Curr Med Chem. 2021;28:1–20. Available from: https://doi.org/10.2174/0929867328666210329094111
17. Tran-Nguyen VK, Camproux A-C. Computational modeling of protein–ligand interactions: From binding site identification to pose prediction and beyond. Curr Opin Struct Biol. 2025;95:103152. doi:10.1016/j.sbi.2025.103152.
18. Ahmed MZ, Hameed S, Ali M, Zaheer A. In silico molecular docking analysis of limonene with the fat mass and obesity-associated protein using AutoDock Vina. Sci J Informatics. 2021;8(1):154-60. Available from: https://doi.org/10.15294/SJI.V8I1.29051
19. Sessa L, Di Biasi L, Parisi R, Concilio S, Piotto S. Receptor flexibility in molecular cross-docking. 2016. doi:10.7287/peerj.preprints.2199v1.
20. Kalita JM, Ghosh S, Sahu S, Dutta M. A statistical analysis to find out an appropriate docking method. Asian J Pharm Clin Res. 2015;8(1):158-160.